Two-dimensional Modelling of a Non-isothermal PROX Reactor with Water Cooling for Fuel Cell Applications

H. Beyer[*1], B. Schönbrod[1], C. Siegel[1], M. Steffen[1] and A. Heinzel[1,2]
[1]Zentrum für BrennstoffzellenTechnik (ZBT) GmbH, Duisburg, Germany
[2]University of Duisburg-Essen, Institut für Energie- und Umweltverfahrenstechnik, Germany
*Corresponding author: Zentrum für BrennstoffzellenTechnik (ZBT) GmbH,
Carl-Benz-Straße 201, D-47057 Duisburg, Germany, h.beyer@zbt-duisburg.de

Abstract: This work treats of a preferential oxidation reactor, which is simulated by a two-dimensional axial symmetric COMSOL Chemical engineering model. The reactor serves as purification of hydrocarbon reformat and converts the CO mole fraction from up to 1 % in the feed gas down to a few ppm at the outlet to deliver a hydrogen rich feed gas for a PEM fuel cell. The model combined chemical kinetic expressions, which were determined within kinetic experiments with mass, energy and momentum transport equations. In a first step the O/CO-ratio was increased successively while the inlet temperature T_0 was held constant. Subsequently the inlet temperature was varied whereas the O/CO-ratio stayed constant. Cross section plots in axial direction are presented and show the reactor performance in terms of reaction temperature, reaction rate, conversion rate and CO mole fraction. The simulations confirmed operability of the model in principle and provided important performance data.

Keywords: Preferential CO oxidation, hydrogen purification, 2D axial symmetry, kinetic expressions

1 Introduction

Steam reforming of hydrocarbons and the use of reformate in PEM fuel cells to generate electricity and heat is well known. Reformer fuel cell assemblies as CHP systems for residential application are in field test state by now. Usually the gas process consists of a reformer and one or more shift stages. The product of the last shift reactor comprises up to 1 % carbon monoxide, which leads to poisoning of the catalyst within the fuel cell electrode. Therefore an additional reactor is necessary to lower the CO content to a few ppm. One possibility is the preferential oxidation process. CO is oxidized by oxygen in a determined O/CO-ratio while hydrogen oxidation has to be minimized. Both reactions are exothermic and the selectivity of the catalyst is very temperature sensitive. CO conversion is best at a low temperature level (80 – 160°C). Hence, a very accurate cooling conception is mandatory, which operates effective even at start and stop procedure, partial load and load change.

This paper describes an annular-gap-shaped PROX reactor with an inner and outer, coaxial cooling equipment (Figure 1). Fuel cell cooling water is used for the PROX cooling [1]. Before reaching the PROX reactor, the educt gas is conditioned in a heat exchanger, which is also fed by fuel cell cooling water. Therefore the cooling water temperature and the educt gas temperature are assumed to be equal.

Figure 1: 3D coaxial reactor design

2 Reaction kinetics

The two main reactions, which take place with the considered catalyst within the observed temperature range are the CO oxidation

$$CO + 0.5 \cdot O_2 \rightarrow CO_2 \qquad \Delta H_R = -283.6\, kJmol^{-1} \qquad (1)$$

and the hydrogen oxidation

$$H_2 + 0.5 \cdot O_2 \rightarrow H_2O \qquad \Delta H_R = -243.5\, kJ \cdot mol^{-1} \qquad (2)$$

The CO and CO_2 methanation reactions and the reverse water gas shift reaction (RWGS), which are mentioned in the literature [2,6] did not occur in the experimental investigations. Hence, they are negligible in the present work. Within a series of kinetic experiments the following two rate

equations (3,4) were determined and used within the Chemical Engineering Module and finally compared with the corresponding literature [2-5]:

$$r_{CO} = 5 \cdot 10^{-5} \cdot \exp\left(\frac{-2.84 \cdot 10^4}{RT}\right) \cdot x_{CO}^{-0.5} \cdot x_{O_2} \quad (3)$$

$$r_{H_2} = 2.6 \cdot 10^{-7} \cdot \exp\left(\frac{-1.8 \cdot 10^4}{RT}\right) \cdot x_{O_2}^{1.16} \quad (4)$$

The mole fraction x_i is defined as the quotient of the species concentration and the total concentration.

$$x_i = \frac{c_i}{c_{total}} \quad (5)$$

3 Use of COMSOL Multiphysics

Due to the axial symmetry of the considered reactor, a 2D geometry is used in COMSOL Multiphysics v3.5a (Figure 2). The mass transport is modeled using a convection and diffusion application mode with the following equation:

$$\nabla \cdot (D_i \nabla c_i) = R_i - u \nabla c_i \quad (6)$$

where c_i (mol m^{-3}) denotes the concentration of the species i, D_i (m^2 s^{-1}) its effective diffusion coefficient, u (m s^{-1}) the velocity vector of the fluid and R_i (mol m^{-3} s^{-1}) the reaction rate. The above mentioned rate expressions (3,4) are implemented as source terms for CO and H_2

$$R_i = -r_i \cdot \quad _{bulk} \qquad i = H_2, CO \quad (7)$$

Due to the required unit mol m^{-3}s^{-1} the reaction rate is multiplied by the bulk density $_{bulk}$. The O_2 reaction rate is defined as

$$R_{O2} = -0.5 \cdot (r_{CO} + r_{H2}) \cdot \quad _{bulk} \quad (8)$$

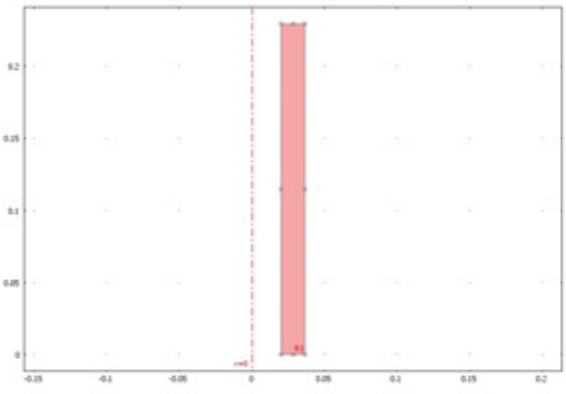

Figure 2: 2D axial symmetric geometry within COMSOL Multiphysics

considering the stoichiometric coefficient. Constant concentrations are used as inlet boundary conditions, whereas a convective flux boundary condition is used at the outlet.

Energy transport is accounted for by using a convective and conductive application mode.

$$\nabla \cdot (-k \cdot \nabla T) = Q - \quad _{gas} \cdot C_p \cdot u \cdot \nabla T \quad (9)$$

where ρ_{gas} (kg m^{-3}) denotes the gas density, C_p (J kg^{-1} K^{-1}) its heat capacity, T (K) the temperature, k (W K^{-1} m^{-1}) the effective thermal conductivity, u (m s^{-1}) the velocity vector of the fluid and Q (J m^{-3} s^{-1}) the heat generation rate per unit volume of the catalyst bed which can be expressed as follows:

$$Q = -\Delta H_{R,CO} \cdot R_{CO} - \Delta H_{R,H2} \cdot R_{H2} \quad (10)$$

The used heat source expression mainly depends on the two rate equations R_i (mol m^{-3} s^{-1}) given above and on the related reaction enthalpies $\Delta H_{R,I}$ (J mol^{-1}). Herein, a constant water temperature is assumed due to the negligible increase in temperature of the cooling medium and its high heat capacity in comparison to the reactants. Therefore a heat flux in the boundary conditions of the two cylindrical walls is defined as follows

$$q_0 = k_w \cdot (T_W - T) \quad (11)$$

where k_w (W m^{-2} K) denotes the heat transfer coefficient across the walls, T_W (K) the temperature of the cooling water, which is assumed to be equal to the inlet temperature T_0, and T (K) the calculated temperature of the reactants.

Due to the catalyst bulk a Brinkman application mode is used (extended Navier-Stokes):

$$- \cdot u = \nabla \left(p \cdot I + \frac{1}{} \left(\quad (\nabla u + (\nabla u)^T) - \frac{2}{3} \quad (\nabla u) I \right) \right) \quad (12)$$

where (Pa s) denotes the dynamic viscosity (m²) the permeability, u (m s^{-1}) the velocity vector, p (Pa) the pressure and the porosity. The inlet flow is assumed to be laminar. At the outlet atmospheric pressure is implied. Due to the spherical shape of the catalyst pellets and the resulting wall effects the porosity follows a radial profile which leads to a velocity distribution depicted in Figure 3.

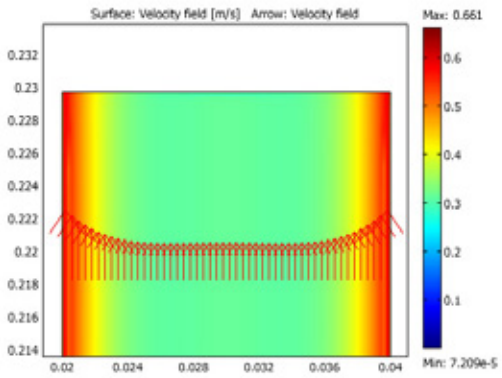

Figure 3: Radial velocity distribution

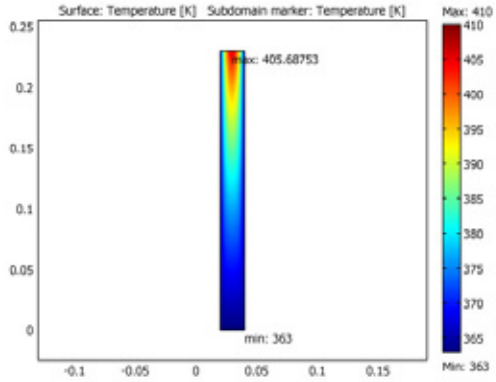

Figure 5: Exemplary surface plot of temperature

The mesh got a rectangular shape (mapped mesh) and was refined at the wall areas by entering a manual edge vertex distribution (Figure 4).

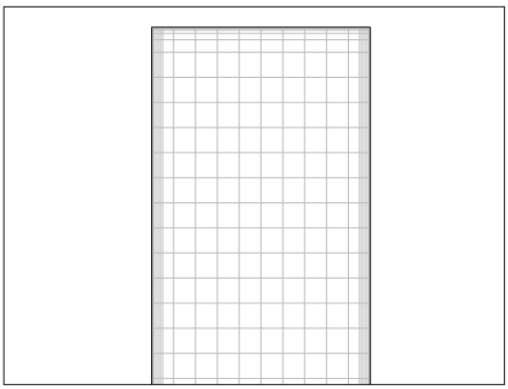

Figure 4: Rectangular mesh

4 Results

A dedicated solver sequence was used in order to obtain a converged solution. Each application mode was solved separately before all three were solved concomitantly. Figure 5 shows a surface plot of the reaction temperature.

Both, an axial and a radial temperature profile are apparent. Furthermore the minimum and the maximum temperature are assigned. In a first step the lambda ratio

$$L = \frac{c_{O_2}}{2 \cdot c_{CO}} \qquad (13)$$

was increased successively from 3.0 to 3.5 while the inlet temperature T_0 was held constant at 363 K. Subsequently the inlet temperature was varied between 343 and 368 K whereas the lambda ratio stayed at 3.0. In the following Figures cross section plots of the temperature T, the reaction rate R_{CO}, the CO conversion rate and the mole fraction are depicted. Increasing lambda ratios lead to weakly increasing outlet temperatures (Figure 6). At a constant lambda ratio the reaction temperature increases more at higher inlet temperatures than at lower (Figure 7). The step-up of the lambda ratio has a higher impact on the reaction rate than the raise in temperature (Figures 8, 9). At higher lambda ratios an exceeding increases of the reaction rate can be observed at the outlet area of the reactor (Figure 8). Figure 10 and Figure 11 illustrate the CO conversion rate distribution in z-direction. The highest conversion rate amounts to 92.5 % at L=3.5, which is not enough to lower the CO mole fraction to a few ppm. Probably an increase in reaction temperature by means of a higher inlet temperature or a geometric improvement leads to a higher CO conversion rate. At reaction temperatures higher than calculated in this work the solver did not converge or result in negative concentrations. The reasons are the Arrhenius and Power Law expressions as source terms in the convection and conduction as well as in the convection and diffusion mode. In Figures 12 and 13 the resulting CO mole fractions are shown. At a lambda ratio 3.0 the lowest value reached about 960 ppm whereas L=3.5 leads to 374 ppm.

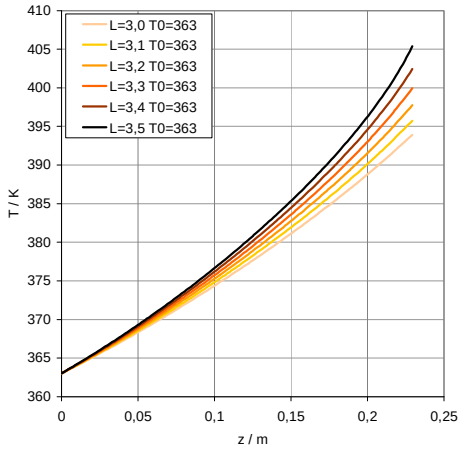

Figure 6: Axial temperature profile T(L,z) at different Lambda values (L) and constant inlet temperature

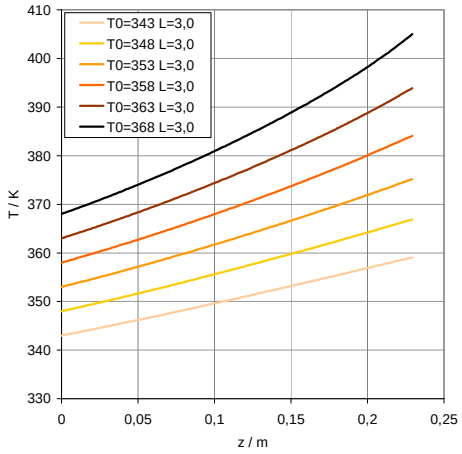

Figure 7: Axial temperature profile T(L,z) at different inlet temperatures and constant Lambda (L)

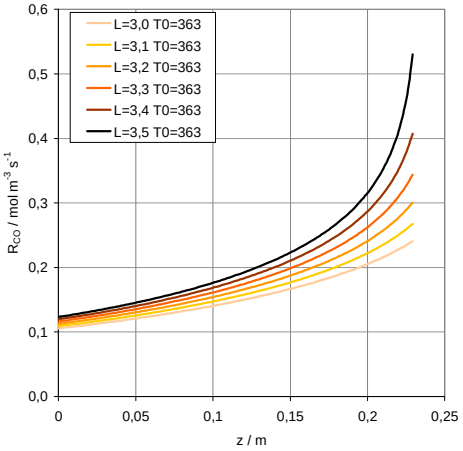

Figure 8: CO reaction rate R_{CO}(L,z)at different Lambda values (L) and constant inlet temperature

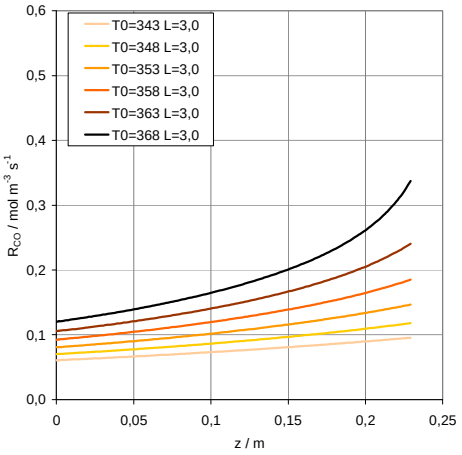

Figure 9: CO reaction rate $R_{CO}(T_0,z)$ at different inlet temperatures and constant Lambda (L)

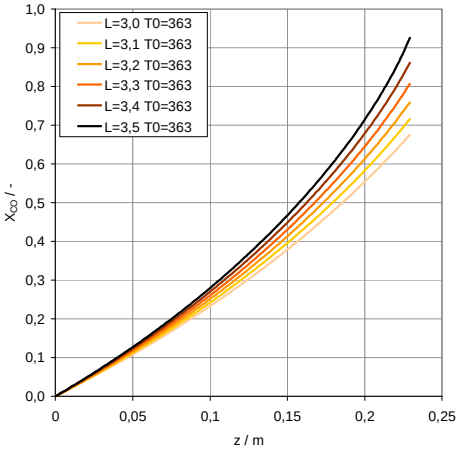

Figure 10: CO conversion rate X_{CO}(L,z) at different Lambda values (L) and constant inlet temperature

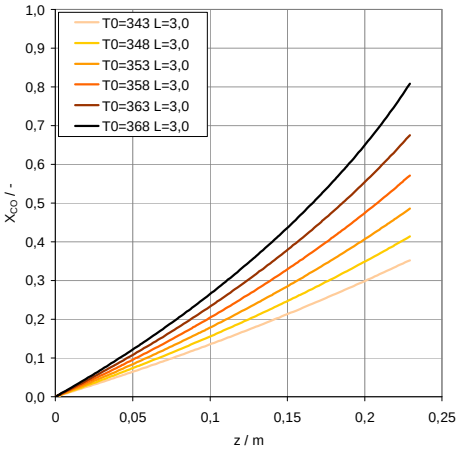

Figure 11: CO conversion rate $X_{CO}(T_0,z)$ at different inlet temperatures and constant Lambda (L)

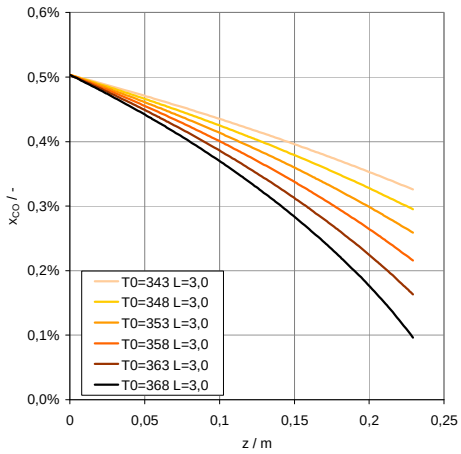

Figure 12: CO mole fraction $x_{CO}(T_0,z)$ at different inlet temperatures and constant Lambda (L)

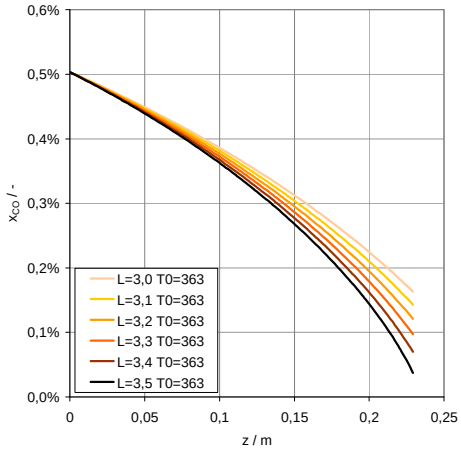

Figure 13: CO mole fraction $x_{CO}(L,z)$ at different Lambda values (L) and constant inlet temperature

5 Conclusion

An annular-gap- PROX reactor with an inner and outer, coaxial cooling equipment was designed and its performance was simulated with Chemical engineering application modes and 2D axial symmetric geometry within COMSOL Multiphysics. The model combined chemical kinetics, which were determined within kinetic experiments with mass, energy and momentum transport phenomena. Two rate equations for the CO oxidation and H_2 oxidation were submitted as source terms in the convection and diffusion mode as well as in the convection and conduction mode respectively. The boundary conditions were adapted to the real reaction conditions.

The simulations confirmed operability of the model in principle and provided important performance data. At a lambda ratio 3.5 the lowest CO mole fraction value reached about 374 ppm with a maximum temperature of about 405 K, which is even lower than in experimental investigations.

At higher reaction temperatures the Simulation did not converge or resulted in negative concentrations. When the CO concentration approaches zero numerical noise becomes significant in comparison to the concentration. For further CO conversion improvement within the model the reaction terms have to be modified such that when the concentration approaches zero so does the reaction rate. Probably a mesh modification or the formulation of logarithmic concentrations can avoid these problems [7].

6 References

[1] H. Beyer, J. Mathiak, Patent DE 10 2006 019 406

[2] Y. Choi, H. G. Stenger, *Kinetics, simulation and insights for CO selective oxidation in fuel cell applications,* Journal of Power Sources 129 (2004) 246-254

[3] M. J. Kahlich, H. A. Gasteiger and R. J. Behm, *Kinetics of the Selective CO Oxidation in H2-Rich Gas on Pt/Al2O3*, Journal of Catalysis 171 (1997) 93–105

[4] E. J. Bisset, S. H. Oh, R. M. Sinkewitch, *Pt surface kinetics for a PrOx reactor for fuel cell feedstream processing*, Chemical Engineering Science 60 (2005) 4709-4721

[5] M. Vahabi, M. H. Akbari, *Three-dimensional simulation and optimization of an isothermal PROX microreactor for fuel cell applications*, Int. Journal of Hydrogen Energy 34 (2009) 1531-1541

[6] F. Cipiti, L. Pino, A. Vita, M. Laganà, V. Recupero, *Modeling of a Preferential Oxidation Reactor in a LPG Hydrogen Generator for PEFC,* Proceedings of the COMSOL Users Conference 2006 Milano

[7] COMSOL Knowledge Base, *Avoiding negative concentrations*, Solution No 952